THE JOURNAL OF PHYSICAL CHEMISTRY C
A JOURNAL OF THE AMERICAN CHEMICAL SOCIETY

pubs.acs.org/JPCC

Article

Impedance Response of Electrochemical Interfaces: Part IV—Low-Frequency Inductive Loop for a Single-Electron Reaction

Published as part of The Journal of Physical Chemistry virtual special issue "Zhao-Wu Tian Festschrift".

Chenkun Li,* Zhangquan Peng, and Jun Huang

Cite This: *J. Phys. Chem. C* 2023, 127, 16367−16373

Read Online

ACCESS | Metrics & More | Article Recommendations | Supporting Information

ABSTRACT: The low-frequency inductive loop is usually attributed to relaxation of adsorbed intermediates of multistep reactions in electrocatalysis and corrosion. Herein, we report a low-frequency inductive loop for a single-electron reaction when the electrode potential (E_M), the equilibrium potential (E_{eq}), and the potential of zero charge (E_{pzc}) are different, namely, under nonequilibrium conditions. Interestingly enough, although both reactions involve only one electron, the metal deposition reaction ($M^+ + e \leftrightarrow M$) and the redox couple reaction ($Fe(CN)_6^{3-} + e \leftrightarrow Fe(CN)_6^{4-}$) show different impedance shapes. The low-frequency inductive loop is observed only for the $M^+ + e \leftrightarrow M$ reaction in the oxidation direction because its faradaic current has a negative phase angle due to double layer effects. Moreover, we find that the low-frequency inductive loop occurs only when the polarization curve has no diffusion-limiting features.

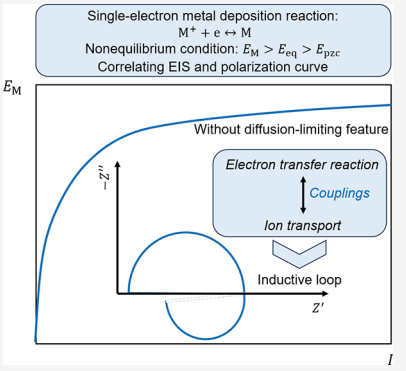

INTRODUCTION

Inductance, widely discussed in the field of electrochemical impedance spectroscopy (EIS), can occur in both high-frequency and low-frequency ranges.[1,2] The high-frequency inductance is usually caused by the electromagnetic interactions of cables in measurements.[2] The low-frequency inductance could be caused by relaxation of adsorbates in multistep reactions in electrocatalysis[3−7] and corrosion,[2,4,8−10] as well as water transport in fuel cells.[11−15]

For reactions including only one electron, such as $Li^+ + e \leftrightarrow Li$ and $Fe(CN)_6^{3-} + e \leftrightarrow Fe(CN)_6^{4-}$, no inductive loop has been reported or is expected since no adsorbate is involved. In our previous study,[16] we found an inductive loop in the low-frequency range for the metal deposition reaction, $M^+ + e \leftrightarrow M$. This inductive loop is observed only under nonequilibrium conditions. In our model, the electron transfer reaction is described using the Frumkin-corrected Butler−Volmer (BV) equation. Electric double layer (EDL) charging and ion transport are described uniformly by the Poisson−Nernst−Planck (PNP) equations. The inductive loop is observed only with a coupling treatment of the electron transfer reaction and the EDL charging.

In this work, we study the mechanism of this inductive loop, explore whether it is a common feature for one-electron reactions under nonequilibrium conditions, and try to correlate the inductive loop in the frequency space with the polarization curve in the time space.

MODEL DEVELOPMENT

We consider two one-electron reactions at a one-dimensional planar electrochemical interface, namely, $M^+ + e \leftrightarrow M$ and $Fe(CN)_6^{3-} + e \leftrightarrow Fe(CN)_6^{4-}$, as shown in Figure 1a,b, respectively. The electrolyte solution is assumed to be dilute.

Ion transport in the electrolyte solution is described by the PNP equations,[17−24]

$$\frac{\partial c_i}{\partial t} + \nabla J_i = 0 \tag{1}$$

$$\nabla^2 \phi = -\frac{F\sum_{i=1}^{n} z_i c_i}{\epsilon_s} \tag{2}$$

where $J_i = -D_i \nabla c_i - \frac{F}{RT} D_i z_i c_i \nabla \phi$ is the flux term, i denotes the cations ($i = +$) or anions ($i = -$), z_i is the charge number, c_i is the concentration, D_i the diffusion coefficient, F is the Faraday constant, R is the ideal gas constant, T is the temperature, and ϵ_s is the permittivity of solution. The PNP equations neglect the ion size effect, short range correlation, and solvent polarization. Extension of PNP equations with one or several limitations released have been developed by Borukhov et al.,[25] Gavish et

Received: April 29, 2023
Revised: July 29, 2023
Published: August 16, 2023

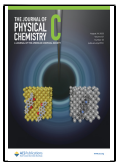

https://doi.org/10.1021/acs.jpcc.3c02830
J. Phys. Chem. C 2023, 127, 16367−16373

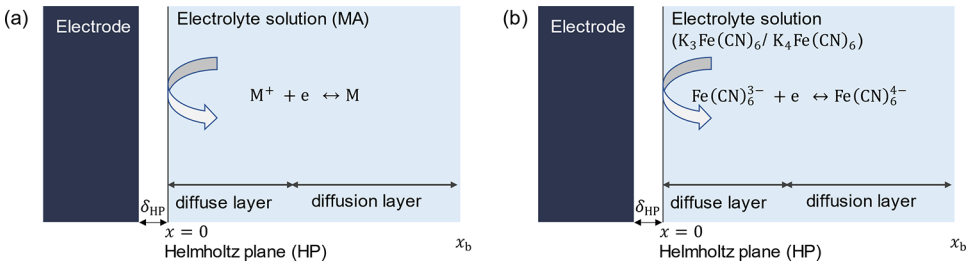

Figure 1. Schematic illustration of the electrochemical interface with a one-electron reaction occurring at the Helmholtz plane (HP), (a) $M^+ + e \leftrightarrow M$ and (b) $Fe(CN)_6^{3-} + e \leftrightarrow Fe(CN)_6^{4-}$.

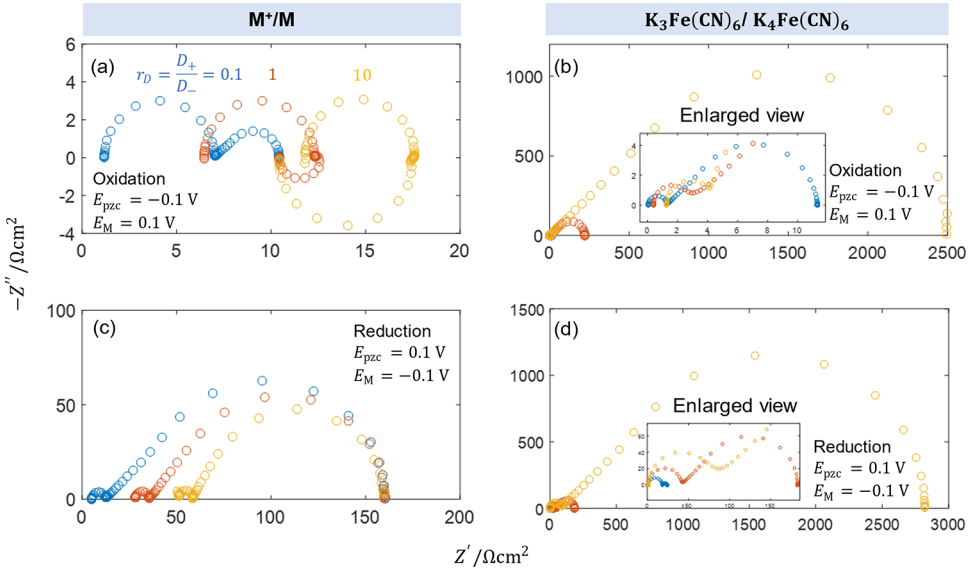

Figure 2. Comparison of electrochemical impedance between the M^+/M reaction in (a) oxidation and (c) reduction directions and the $Fe(CN)_6^{3-}/Fe(CN)_6^{4-}$ reaction in (b) oxidation and (d) reduction directions under the conditions of $E_M \neq E_{eq} \neq E_{pzc}$, E_{eq} is taken as the potential reference. Parameters used in calculation are as follows: $c_0 = 0.1$ mol L^{-1}, $D_+ = 1 \times 10^{-10}$ m^2 s^{-1}, $r_D = D_+/D_-$ by changing D_- only, $k_0 = 3 \times 10^{-4}$ m^2 s^{-1}, $x_b = 100$ μm, and a frequency range from 500 kHz to 0.01 mHz.

al.,[26,27] Liu and Eisenberg,[28] de Souza and Bazant,[29] and also ourselves.[30,31] We expect that these more complications will not change the shape of the EIS curve.

For the left boundary, the flux of ions included in the reaction is correlated with the reaction current density. The reaction rate is described using the Frumkin-corrected BV equation,[16,32] with the current density positive-defined for the oxidation reaction per the IUPAC convention,[33]

$$J_{M^+} = k_0\left(\exp\left(\frac{\alpha F\eta}{RT}\right) - \frac{c_{M^+,HP}}{c^0_{M^+}}\exp\left(-\frac{(1-\alpha)F\eta}{RT}\right)\right) \quad (3)$$

for the M^+/M reaction and

$$J_{Fe(CN)_6^{3-}} = k_0\left(\frac{c_{Fe(CN)_6^{4-},HP}}{c^0_{Fe(CN)_6^{4-}}}\exp\left(\frac{\alpha F\eta}{RT}\right) - \frac{c_{Fe(CN)_6^{3-},HP}}{c^0_{Fe(CN)_6^{3-}}}\exp\left(-\frac{(1-\alpha)F\eta}{RT}\right)\right) \quad (4)$$

$$J_{Fe(CN)_6^{4-}} = -k_0\left(\frac{c_{Fe(CN)_6^{4-},HP}}{c^0_{Fe(CN)_6^{4-}}}\exp\left(\frac{\alpha F\eta}{RT}\right) - \frac{c_{Fe(CN)_6^{3-},HP}}{c^0_{Fe(CN)_6^{3-}}}\exp\left(-\frac{(1-\alpha)F\eta}{RT}\right)\right) \quad (5)$$

for the $Fe(CN)_6^{3-}/Fe(CN)_6^{4-}$ reaction, where k_0 is the rate constant, $c_{M^+,HP}$, $c_{Fe(CN)_6^{3-},HP}$, and $c_{Fe(CN)_6^{4-},HP}$ are the concentration of M^+, $Fe(CN)_6^{3-}$, and $Fe(CN)_6^{4-}$ at the HP, the superscript "0" denotes their bulk values, α the transfer coefficient, and η the local overpotential defined as,

$$\eta = E_M - \phi_{HP} - E_{eq} \quad (6)$$

where E_M is the electrode potential, E_{eq} is the equilibrium potential, and ϕ_{HP} is the potential at the HP.

Ions not involved in reactions have a zero flux,

$$J_{A^-} = 0 \quad (7)$$

$$J_{K^+} = 0 \quad (8)$$

where A^- denotes an arbitrary monovalent anion, K^+ denotes the potassium ion.

Here, we assume that the reaction occurs at the HP, and there is no space charge between the electrode surface and the HP.

https://doi.org/10.1021/acs.jpcc.3c02830
J. Phys. Chem. C 2023, 127, 16367−16373

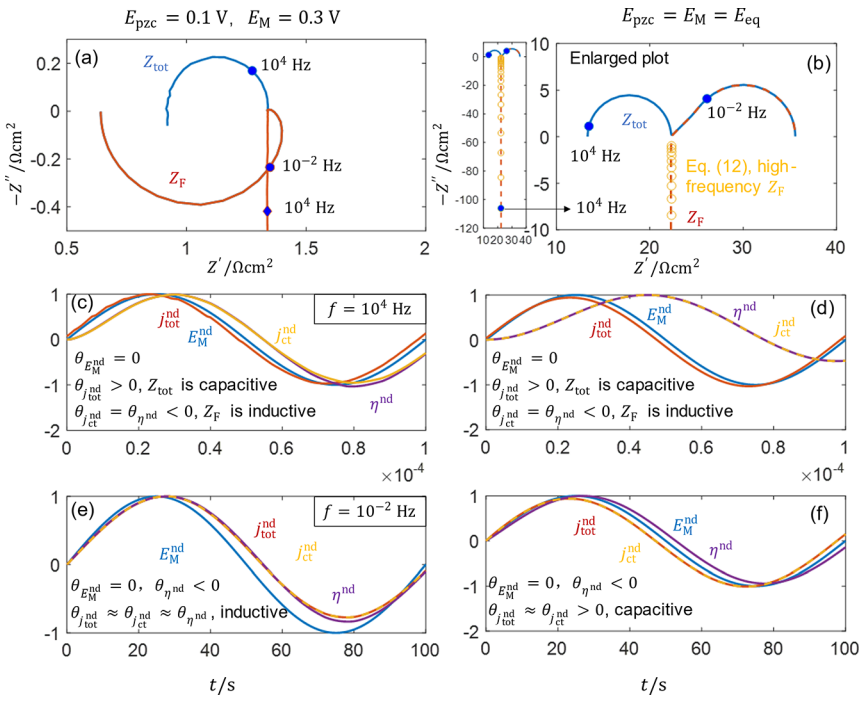

Figure 3. Comparison between the total impedance Z_{tot} and Faradaic impedance Z_F in (a) and (b), the time-domain signals E_M^{nd}, j_{tot}^{nd}, j_{ct}^{nd}, and η^{nd} at 10^4 Hz in (c) and (d), and 10^{-2} Hz in (e) and (f) under the conditions of E_{pzc} = 0.1 V, E_M = 0.3 V, and E_M = E_{eq} = E_{pzc}. Parameters used in calculation are as follows: D_+ = D_- = 1 × 10^{-10} m^2 s^{-1}, others are the same as those used in Figure 2.

Therefore, the electric potential is linear in the space between the electrode surface and the HP,

$$\phi_{HP} = E_M - E_{pzc} + \frac{\epsilon_S \delta_{HP}}{\epsilon_{HP}} \frac{\partial \phi}{\partial x} \tag{9}$$

where E_{pzc} is the potential of zero charge (PZC), ϵ_{HP} is the dielectric permittivity in the space between the electrode surface and the HP, and δ_{HP} is the distance from the electrode surface to the HP, respectively.

For the right boundary, which is located at the bulk solution, x = x_b, all ions have their bulk concentrations, and the electric potential is zero, namely,

$$c_{M^+} = c_{M^+}^0,\ c_{A^-} = c_{A^-}^0,\ c_{K^+} = c_{K^+}^0\ c_{Fe(CN)_6^{3-}} = c_{Fe(CN)_6^{3-}}^0\ ,\ c_{Fe(CN)_6^{4-}} = c_{Fe(CN)_6^{4-}}^0,\ \phi = 0 \tag{10}$$

The total impedance Z_{tot} is defined as the ratio of the Fourier-transformed (FT) electrode potential E_M over the FT total current density j_{tot},[16,34]

$$Z_{tot} = \frac{FT(E_M)}{FT(j_{tot})} \tag{11}$$

where j_{tot} is the sum of reaction current density j_{ct} and EDL current density j_{dl}, j_{tot} = j_{ct} + j_{dl}. The workflow of numerical solution is inherited from our previous work,[16] and the modifications are detailed in Section 1 of the Supporting Information.

RESULTS AND DISCUSSION

In this section, we first compare the impedance between the $M^+ + e \leftrightarrow M$ reaction and the $Fe(CN)_6^{3-} + e \leftrightarrow Fe(CN)_6^{4-}$ reaction under the conditions of $E_M \neq E_{eq} \neq E_{pzc}$. Second, we give a mechanistic interpretation for the low-frequency inductive loop by decomposing the time-domain signals. Lastly, we correlate the EIS and polarization curve and then further clarify the necessary conditions for the appearance of an inductive loop.

Comparison of Impedance between the M^+/M Reaction and the $Fe(CN)_6^{3-}$/$Fe(CN)_6^{4-}$ Reaction. Figure 2 compares the impedance between the M^+/M reaction and the $Fe(CN)_6^{3-}$/$Fe(CN)_6^{4-}$ reaction under the conditions of $E_M \neq E_{eq} \neq E_{pzc}$. We notice that for the M^+/M reaction, the low-frequency inductive loop only occurs in the oxidation process, and its size increases with increasing r_D, which is the ratio between D_+ and D_-, r_D = D_+/D_-. Here, we fix D_+ and only change D_- when simulating the effect of r_D. Therefore, we conclude that decreasing D_- slows down the total transport process and promotes the occurrence of the inductive loop. Previous works on anodic dissolution of metals, following a two-electron mechanism, also observed the anion effect on the inductive loop.[35,36] In their studies, the inductive loop is caused by the diffusion rate faster than the second electron transfer. Our model can also be extended to multiple-electron transfer reactions by considering multistep reaction kinetics. Herein, we focus on the one-electron reaction. For the reduction process of the M^+/M reaction shown in Figure 2c, there is no inductive loop. The low-frequency semicircle represents ion transport in a finite-length space. For both oxidation and reduction processes, the high-frequency semicircle represents charge transfer reaction.

For the $Fe(CN)_6^{3-}$/$Fe(CN)_6^{4-}$ reaction, there is no inductive loop in both oxidation and reduction processes. Since we set E_{eq} as a reference, oxidation occurs when $E_M > E_{eq}$ and reduction occurs when $E_M < E_{eq}$. The low-frequency semicircle also represents ion transport in a finite-length space. We notice that the low-frequency semicircle increases with increasing r_D because we change r_D by fixing D_+ and decreasing D_-. Cautious readers may notice that the high-frequency semicircle in Figure 2b is almost invisible. This is due to the fact that larger η causes a

https://doi.org/10.1021/acs.jpcc.3c02830
J. Phys. Chem. C 2023, 127, 16367−16373

smaller $R_{ct} \approx \frac{RT}{\alpha F j_0}\exp\left(-\frac{\alpha F}{RT}\eta\right)$ with j_0 being the exchange current density.

For both M^+/M and $Fe(CN)_6^{3-}/Fe(CN)_6^{4-}$ reactions, the high-frequency solution resistance increases with increasing r_D, which is realized by fixing D_+ and decreasing D_-. This is because the solution conductivity decreases at reduced D_-. The mechanistic interpretation of the inductive loop for the M^+/M reaction will be given in the next section.

Mechanistic Interpretation for the Low-Frequency Inductive Loop. The low-frequency inductive loop means that the imaginary part Z' is larger than zero, and the phase angle of impedance is positive. If the applied electrode potential is a zero-phase angle signal, then we conclude that the phase angle of total current density j_{tot} is negative, $\theta_{j_{tot}} < 0$. In the low-frequency range, $j_{dl} \ll j_{ct}$, which means that the inductive loop comes from j_{ct}. For the oxidation reaction with a large positive overpotential η, the Frumkin-corrected BV equation in eq 3 can be approximated to $J_{M^+} \approx k_0\exp\left(\frac{\alpha F\eta}{RT}\right)$. Considering the linear assumption of impedance, we obtain $\tilde{J}_{M^+} \approx \overline{J}_{M^+}\frac{\alpha F}{RT}\tilde{\eta}$, with "~" representing small-perturbation variables and $\overline{J}_{M^+} = k_0\exp\left(\frac{\alpha F\overline{\eta}}{RT}\right)$ representing the stationary values. Therefore, we conclude that $\theta_{j_{tot}}$ and θ_η are the same in the low-frequency range.

To validate the above theoretical analysis, Figure 3a,b first compare the total impedance Z_{tot} and Faradaic impedance Z_F defined as $Z_F = \frac{FT(E_M)}{FT(j_{ct})}$ of the M^+/M reaction under the conditions of $E_M \neq E_{eq} \neq E_{pzc}$ and $E_M = E_{eq} = E_{pzc}$, respectively. Then, we compare time-domain signals at 10^4 Hz and 10^{-2} Hz to understand the impedance response.

For the case of $E_M \neq E_{eq} \neq E_{pzc}$, Figure 3a first compares Z_{tot} and Z_F at 10^4 Hz and 10^{-2} Hz. We find that the low-frequency regions of Z_{tot} and Z_F coincide, and the high-frequency regions have large differences since j_{dl} dominates over j_{ct} in a high-frequency range, which agrees with our theoretical analysis. Unexpectedly, Z_F is inductive in the high-frequency range. We usually regard Z_F as a series of charge transfer resistance and mass transport impedance in the classical Randles circuit model.[4] Figure 3c compares the time-domain signals of E_M^{nd}, j_{tot}^{nd}, j_{ct}^{nd}, and η^{nd} at 10^4 Hz, where the superscript "nd" denotes dimensionless variables normalized by their maximum values, respectively. We find that $\theta_{j_{tot}^{nd}} > 0$, Z_{tot} is capacitive, while $\theta_{j_{ct}^{nd}} < 0$, Z_F is inductive. Similarly, Figure 3e compares the time-domain signals of E_M^{nd}, j_{tot}^{nd}, j_{ct}^{nd}, and η^{nd} at 10^{-2} Hz. We find that $\theta_{j_{tot}^{nd}} \approx \theta_{j_{ct}^{nd}} \approx \theta_{\eta^{nd}} < 0$, both Z_{tot} and Z_F are inductive, which also agrees with our theoretical analysis.

For the case of $E_M = E_{eq} = E_{pzc}$, Figure 3b compares Z_{tot} and Z_F at 10^4 Hz and 10^{-2} Hz. Z_{tot} and Z_F also coincide in the low-frequency range and have large differences in the high-frequency range. We notice that Z_F is also inductive in the high-frequency range, which is the same as that under the conditions of $E_M \neq E_{eq} \neq E_{pzc}$. Since this feature occurs under both conditions of $E_M = E_{eq} = E_{pzc}$ and $E_M \neq E_{eq} \neq E_{pzc}$, we conclude that the inductive feature of Z_F is intrinsic and caused by EDL effects.

To validate the above analysis, we derive an approximate solution of Z_F in high frequency under the condition of $E_M = E_{eq} = E_{pzc}$ (the detailed derivation is given in Section 3 of the Supporting Information),

$$Z_F = R_{ohm} + R_{ct} + \frac{\chi_1 R_{ct}^2\frac{DC_{GC}}{\lambda_D^2} + \chi_2\frac{\lambda_D^2}{DC_{GC}} + \chi_3 R_{ct}}{\chi_4 + \chi_5 R_{ct}\frac{DC_{GC}}{2\lambda_D^2}} \tag{12}$$

where $R_{ohm} = \frac{\lambda_D^2}{DC_{GC}}X_b$ is the bulk solution resistance with $\lambda_D = \sqrt{\frac{\epsilon_s RT}{2F^2 c_0}}$ being the Debye length, $X_b = x_b/\lambda_D$ is the dimensionless electrolyte thickness, $C_{GC} = \frac{\epsilon_s}{\lambda_D}$ is the Gouy–Chapman capacitance at the PZC, $R_{ct} = \frac{RT}{F^2 k_0}$ is the charge transfer resistance, and

$$\chi_1 = j\omega^{nd}(X_b - r_c) + \left(\sqrt{j\omega^{nd}} + \frac{1}{\sqrt{j\omega^{nd}}}\frac{r_c+1}{X_b} - r_c\frac{r_c+1}{X_b}\right) \tag{13}$$

$$\chi_2 = (1 - r_c - r_c^2 - r_c\sqrt{j\omega^{nd}})X_b - r_c\frac{r_c+1}{\sqrt{j\omega^{nd}}} + \frac{r_c+1}{j\omega^{nd}} \tag{14}$$

$$\chi_3 = \sqrt{j\omega^{nd}}(2X_b - r_c) + \frac{1}{\sqrt{j\omega^{nd}}}\left(2(r_c+1) - r_c\frac{r_c+1}{X_b}\right) + (1 - 2r_c - 2r_c^2) + \frac{1}{j\omega^{nd}}\frac{r_c+1}{X_b} - j\omega^{nd}r_c X_b \tag{15}$$

$$\chi_4 = r_c + r_c^2 - 1 - \frac{1+r_c}{X_b} + r_c\left(\frac{1+r_c}{X_b}\frac{1}{\sqrt{j\omega^{nd}}} + \sqrt{j\omega^{nd}}\right) \tag{16}$$

$$\chi_5 = 2r_c\left(\frac{r_c+1}{X_b} + j\omega^{nd}\right) - 2\left(\frac{r_c+1}{X_b}\frac{1}{\sqrt{j\omega^{nd}}} + \sqrt{j\omega^{nd}}\right) + 2r_c + 2 \tag{17}$$

with $\omega^{nd} = \omega D/\lambda_D^2$ being the dimensionless angular frequency, r_c is the ratio between C_{GC} and Helmholtz capacitance $C_H = \frac{\epsilon_{HP}}{\delta_{HP}}$.

In conventional wisdom, the third term in eq 12 should be zero. However, in the present analysis, it is a complicated combination of R_{ct}, C_{GC}, and other factors, which causes a high-frequency inductance. Figure 3b compares the results of Z_{tot} (blue solid line), Z_F (orange dash line) and eq 12 (yellow circles). Equation 12 and Z_F coincide in high frequency, which agrees with our theoretical analysis. This is a fingerprint of couplings between the charge transfer reaction and EDL dynamics.[16]

Figure 3d compares the time-domain signals of E_M^{nd}, j_{tot}^{nd}, j_{ct}^{nd}, and η^{nd} at 10^4 Hz. We find that if $\theta_{j_{ct}^{nd}} \approx \theta_{\eta^{nd}} < 0$, then Z_F is inductive. For the low-frequency inductive loop, Figure 3f compares the time-domain signals of E_M^{nd}, j_{tot}^{nd}, j_{ct}^{nd}, and η^{nd} at 10^{-2} Hz. We find that although $\theta_{\eta^{nd}} < 0$ and $\theta_{j_{tot}^{nd}} \approx \theta_{j_{ct}^{nd}} > 0$, Z_F and Z_{tot} coincide and are capacitive, which indicates that the second term

https://doi.org/10.1021/acs.jpcc.3c02830
J. Phys. Chem. C 2023, 127, 16367−16373

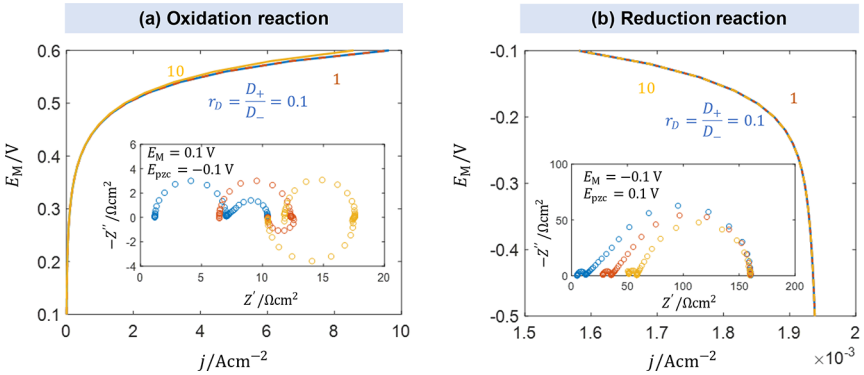

Figure 4. Comparison of polarization curves between oxidation (a) and reduction (b) processes for the M^+/M reaction. The lines and circles with different colors denote the influence of $r_D = D_+/D_-$. Other parameters used in calculation are the same as those in Figure 2.

$k_0 \frac{c_{M^+,HP}}{c^0_{M^+}} \exp\left(-\frac{(1-\alpha)F\eta}{RT}\right)$ in eq 3 cannot be neglected under the conditions of $E_M = E_{eq} = E_{pzc}$.

For the $Fe(CN)_6^{3-}/Fe(CN)_6^{4-}$ reaction, the analysis of time-domain signals is provided in Section 2 of the Supporting Information. There is no low-frequency inductive loop for the $Fe(CN)_6^{3-}/Fe(CN)_6^{4-}$ reaction, and $\theta^{nd}_{j_{tot}}$ is always positive in the whole frequency range. The high-frequency part of Z_F also shows an inductance for both oxidation and reduction processes, which is the same as that in the M^+/M reaction.

Correlating the EIS and Polarization Curve. Herein, we want to know whether there is a signal of the inductive loop in the polarization curves. Figure 4 compares the polarization curves between oxidation and reduction processes for the M^+/M reaction. We recall that the inductive loop is found only in the oxidation direction, see Figure 2. We find that the polarization curve has no diffusion-limiting current density for the oxidation process, while for the reduction process, there is an obvious diffusion-limiting current density.

For the oxidation reaction, the Frumkin-corrected BV equation can be approximated to $J_{M^+} \approx k_0 \exp\left(\frac{\alpha F\eta}{RT}\right)$. We notice that there is no concentration term in the front of the exponential terms, and there is no diffusion-limiting current density in the polarization curve. For the reduction reaction, the Frumkin-corrected BV equation can be approximated to $J_{M^+} \approx k_0 \frac{c_{M^+,HP}}{c^0_{M^+}} \exp\left(-\frac{(1-\alpha)F\eta}{RT}\right)$. There is a concentration term $\frac{c_{M^+,HP}}{c^0_{M^+}}$ in the front of the exponential terms, which means that the diffusion-limiting current density exists in the polarization curve.

For the oxidation reaction, the Nyquist plot in Figure 4a shows that with increasing r_D, the low-frequency resistance is even lower than the high-frequency solution resistance. For the reduction reaction, the Nyquist plot in Figure 4b shows that with increasing r_D, the low-frequency resistance is almost unchanged and the semicircle decreases, which agrees with the analytical solution under the conditions of $E_M = E_{eq} = E_{pzc}$ in our previous work.[16] In addition, we find that the polarization curve has a little difference under different r_D values, while the impedance has a large difference, which shows that the impedance is more sensitive to variations in parameters.

For the $Fe(CN)_6^{3-}/Fe(CN)_6^{4-}$ reaction, the comparison of polarization curves between oxidation and reduction processes is provided in Section 3 of the Supporting Information. There is an obvious diffusion-limiting current density in the polarization curve for both oxidation and reduction. This is because there is always a concentration term in the front of the exponential terms in eqs 4 and 5.

In an experimental study on $Ag^+ + e \leftrightarrow Ag$, with an electrolyte solution of 1 M $AgNO_3$ + 0.5 M HNO_3, an inductive loop was also observed under nonequilibrium conditions with a current of 1 mA.[37] The inductive loop was ascribed to nucleation and growth of Ag.[37] Herein, our model provides an alternative interpretation, which attributes it to the couplings between the charge transfer reaction and ion transport under nonequilibrium conditions. A combination of both the coupling and the nucleation-growth process will be helpful to explore the contribution of each contribution under a wide range of conditions.

CONCLUSIONS

In this work, we present a theoretical analysis of the impedance response of both oxidation and reduction processes of the metal deposition reaction ($M^+ + e \leftrightarrow M$) and the redox couple reaction ($Fe(CN)_6^{3-} + e \leftrightarrow Fe(CN)_6^{4-}$). The electron transfer reaction is described using the Frumkin-corrected BV theory. EDL charging and ion transport are described uniformly using the PNP theory. Different electrode potentials (E_M), equilibrium potentials (E_{eq}), potential of zero charges (E_{pzc}), namely, $E_M \neq E_{eq} \neq E_{pzc}$, and diffusion coefficients for cations and anions ($D_+ \neq D_-$) are considered.

We find that the low-frequency inductive loop only occurs in the oxidation process of the M^+/M reaction where the polarization curve has no diffusion-limiting features. The decomposition of time-domain signals shows that the negative phase angle of Faradaic current density causes the inductive loop.

In addition, we find that the Faradaic impedance always shows the inductance feature in the high-frequency range for both M^+/M and $Fe(CN)_6^{3-}/Fe(CN)_6^{4-}$ in both oxidation and reduction directions, which is revealed to be a fingerprint of EDL effects on the electron transfer reaction. However, the EDL current density dominates in the high-frequency range, muting the inductance in the total impedance.

ASSOCIATED CONTENT

Supporting Information

The Supporting Information is available free of charge at https://pubs.acs.org/doi/10.1021/acs.jpcc.3c02830.

Workflow of the numerical solution, analysis of time-domain signals for the $Fe(CN)_6^{3-}/Fe(CN)_6^{4-}$ reaction, derivation of an approximate solution of Faradaic

https://doi.org/10.1021/acs.jpcc.3c02830
J. Phys. Chem. C 2023, 127, 16367−16373

impedance in the high-frequency limit, and comparison of polarization curves between oxidation and reduction processes for the $Fe(CN)_6^{3-}/Fe(CN)_6^{4-}$ reaction (PDF)

AUTHOR INFORMATION

Corresponding Author

Chenkun Li − *Institute of Energy and Climate Research (IEK-13), Forschungszentrum Jülich, 52425 Jülich, Germany;* orcid.org/0000-0001-5574-0805; Email: ch.li@fz-juelich.de

Authors

Zhangquan Peng − *Laboratory of Advanced Spectro-Electrochemistry and Lithium-Ion Batteries, Dalian National Laboratory for Clean Energy, Dalian Institute of Chemical Physics, Chinese Academy of Sciences, Dalian 116023, China;* orcid.org/0000-0002-4338-314X

Jun Huang − *Institute of Energy and Climate Research (IEK-13), Forschungszentrum Jülich, 52425 Jülich, Germany; Chair of Theory and Computation of Energy Materials, Faculty of Georesources and Materials Engineering, RWTH Aachen University, 52062 Aachen, Germany;* orcid.org/0000-0002-1668-5361

Complete contact information is available at: https://pubs.acs.org/10.1021/acs.jpcc.3c02830

Notes

The authors declare no competing financial interest.

ACKNOWLEDGMENTS

J.H. acknowledges the Initiative and Networking Fund of the Helmholtz Association (No. VH-NG-1709). Z.P. acknowledges the financial support from the National Natural Science Foundation of China (21972055, 22232005, and 21825202), Newton Advanced Fellowships (NAF/R2/180603), and "Scientist Studio Funding" from Tianmu Lake Institute of Advanced Energy Storage Technologies Co., Ltd.

REFERENCES

(1) Huang, J.; Gao, Y.; Luo, J.; Wang, S.; Li, C.; Chen, S.; Zhang, J. Review—Impedance Response of Porous Electrodes: Theoretical Framework, Physical Models and Applications. *J. Electrochem. Soc.* **2020**, *167*, No. 166503.

(2) Wang, S.; Zhang, J.; Gharbi, O.; Vivier, V.; Gao, M.; Orazem, M. E. Electrochemical Impedance Spectroscopy. *Nat. Rev. Methods Primers* **2021**, *1*, 41.

(3) Electrochemical Impedance Spectroscopy for Electrocatalytic Interfaces and Reactions: Classics Never Die. *J. Electrochem.* **2020**, *26*, 3−18, DOI: 10.13208/j.electrochem.181245.

(4) Lasia, A. *Electrochemical Impedance Spectroscopy and Its Applications*; Springer, 2014; pp 143−248.

(5) Harrington, D. A.; Conway, B. Ac Impedance of Faradaic Reactions Involving Electrosorbed Intermediates—I. Kinetic Theory. *Electrochim. Acta* **1987**, *32*, 1703−1712.

(6) Schouler, E.; Kleitz, M. Electrocatalysis and Inductive Effects at the Gas, Pt/Stabilized Zirconia Interface. *J. Electrochem. Soc.* **1987**, *134*, 1045.

(7) Bai, L.; Conway, B. Complex Behavior of Al Dissolution in Non-Aqueous Medium as Revealed by Impedance Spectroscopy. *J. Electrochem. Soc.* **1990**, *137*, 3737.

(8) Mansfeld, F. Models for the Impedance Behavior of Protective Coatings and Cases of Localized Corrosion. *Electrochim. Acta* **1993**, *38*, 1891−1897.

(9) Zhang, G.; Cheng, Y. Corrosion of X65 Steel in Co2-Saturated Oilfield Formation Water in the Absence and Presence of Acetic Acid. *Corros. Sci.* **2009**, *51*, 1589−1595.

(10) Jingling, M.; Jiuba, W.; Gengxin, L.; Chunhua, X. The Corrosion Behaviour of Al−Zn−in−Mg−Ti Alloy in NaCl Solution. *Corros. Sci.* **2010**, *52*, 534−539.

(11) Yuan, X.; Wang, H.; Sun, J. C.; Zhang, J. Ac Impedance Technique in Pem Fuel Cell Diagnosis—a Review. *Int. J. Hydrogen Energy* **2007**, *32*, 4365−4380.

(12) Pivac, I.; Barbir, F. Inductive Phenomena at Low Frequencies in Impedance Spectra of Proton Exchange Membrane Fuel Cells−a Review. *J. Power Sources* **2016**, *326*, 112−119.

(13) Wiezell, K.; Gode, P.; Lindbergh, G. Steady-State and Eis Investigations of Hydrogen Electrodes and Membranes in Polymer Electrolyte Fuel Cells: I. Modeling. *J. Electrochem. Soc.* **2006**, *153*, A749.

(14) Wiezell, K.; Gode, P.; Lindbergh, G. Steady-State and EIS Investigations of Hydrogen Electrodes and Membranes in Polymer Electrolyte Fuel Cells: II. Experimental. *J. Electrochem. Soc.* **2006**, *153*, A759.

(15) Schneider, I.; Bayer, M.; Wokaun, A.; Scherer, G. Impedance Response of the Proton Exchange Membrane in Polymer Electrolyte Fuel Cells. *J. Electrochem. Soc.* **2008**, *155*, B783.

(16) Li, C. K.; Zhang, J.; Huang, J. Impedance Response of Electrochemical Interfaces. Iii. Fingerprints of Couplings between Interfacial Electron Transfer Reaction and Electrolyte-Phase Ion Transport. *J. Chem. Phys.* **2022**, *157*, 184704.

(17) Macdonald, J. R. Theory of Space-Charge Polarization and Electrode-Discharge Effects. *J. Chem. Phys.* **1973**, *58*, 4982−5001.

(18) Brumleve, T. R.; Buck, R. P. Numerical Solution of the Nernst-Planck and Poisson Equation System with Applications to Membrane Electrochemistry and Solid State Physics. *J. Electroanal. Chem. Interfacial Electrochem.* **1978**, *90*, 1−31.

(19) Jamnik, J.; Maier, J. Treatment of the Impedance of Mixed Conductors Equivalent Circuit Model and Explicit Approximate Solutions. *J. Electrochem. Soc.* **1999**, *146*, 4183.

(20) Jamnik, J.; Maier, J. Generalised Equivalent Circuits for Mass and Charge Transport: Chemical Capacitance and Its Implications. *Phys. Chem. Chem. Phys.* **2001**, *3*, 1668−1678.

(21) Lai, W.; Haile, S. M. Impedance Spectroscopy as a Tool for Chemical and Electrochemical Analysis of Mixed Conductors: A Case Study of Ceria. *J. Am. Ceram. Soc.* **2005**, *88*, 2979−2997.

(22) Balu, B.; Khair, A. S. The Electrochemical Impedance Spectrum of Asymmetric Electrolytes across Low to Moderate Frequencies. *J. Electroanal. Chem.* **2022**, *911*, No. 116222.

(23) Li, C. K.; Huang, J. Impedance Response of Electrochemical Interfaces: Part I. Exact Analytical Expressions for Ideally Polarizable Electrodes. *J. Electrochem. Soc.* **2021**, *167*, No. 166517.

(24) Zhang, L.-L.; Li, C.-K.; Huang, J. A Beginners' Guide to Modelling of Electric Double Layer under Equilibrium, Nonequilibrium and Ac Conditions. *J. Electrochem.* **2022**, *28*, No. 2108471.

(25) Borukhov, I.; Andelman, D.; Orland, H. Steric Effects in Electrolytes: A Modified Poisson-Boltzmann Equation. *Phys. Rev. Lett.* **1997**, *79*, 435.

(26) Gavish, N.; Elad, D.; Yochelis, A. From Solvent-Free to Dilute Electrolytes: Essential Components for a Continuum Theory. *J. Phys. Chem. Lett.* **2018**, *9*, 36−42.

(27) Gavish, N. Poisson−Nernst−Planck Equations with High-Order Steric Effects. *Phys. D* **2020**, *411*, No. 132536.

(28) Liu, J.-L.; Eisenberg, B. Molecular Mean-Field Theory of Ionic Solutions: A Poisson-Nernst-Planck-Bikerman Model. *Entropy* **2020**, *22*, 550.

(29) de Souza, J. P.; Bazant, M. Z. Continuum Theory of Electrostatic Correlations at Charged Surfaces. *J. Phys. Chem. C* **2020**, *124*, 11414−11421.

(30) Zhang, Z.; Gao, Y.; Chen, S.; Huang, J. Understanding Dynamics of Electrochemical Double Layers Via a Modified Concentrated Solution Theory. *J. Electrochem. Soc.* **2019**, *167*, No. 013519.

(31) Zhang, L.; Cai, J.; Chen, Y.; Huang, J. Modelling Electrocatalytic Reactions with a Concerted Treatment of Multistep Electron Transfer

Kinetics and Local Reaction Conditions. *J. Phys.: Condens. Matter* **2021**, *33*, 504002.
(32) Bard, A. J.; Faulkner, L. R.; White, H. S. *Electrochemical Methods: Fundamentals and Applications*; John Wiley & Sons, 2022; pp 92−99.
(33) Pingarrón, J. M.; Labuda, J.; Barek, J.; Brett, C. M. A.; Camões, M. F.; Fojta, M.; Hibbert, D. B. Terminology of Electrochemical Methods of Analysis (IUPAC Recommendations 2019). *Pure Appl. Chem.* **2020**, *92*, 641−694.
(34) Xiang Li, Q.-A. H.; Li, W.-H.; Bai, Y.-X.; Wang, J.; Liu, Y.; Zhao, Y.-F.; Wang, J.; Zhang, J.-J. Fundamentals of Electrochemical Impedance Spectroscopy for Macrohomogeneous Porous Electrodes. *J. Electrochem.* **2021**, *27*, 467−497.
(35) García-Jareño, J.; Giménez-Romero, D.; Keddam, M.; Vicente, F. Graphical Analysis of Electrochemical Impedance Spectroscopy of Two Consecutive Irreversible Electron Transfers. 1. Theoretical Study of the Anodic Dissolution of Metals. *J. Phys. Chem. B* **2005**, *109*, 4584−4592.
(36) García-Jareño, J.; Giménez-Romero, D.; Keddam, M.; Vicente, F. Graphical Analysis of Electrochemical Impedance Spectroscopy of Two Consecutive Irreversible Electron Transfers. 2. Zinc Anodic Dissolution in Acid Media. *J. Phys. Chem. B* **2005**, *109*, 4593−4598.
(37) Cachet, C.; Epelboin, I.; Keddam, M.; Wiart, R. The Ag/Ag+ System: An Impedance Model for Nucleation and Growth. *J. Electroanal. Chem. Interfacial Electrochem.* **1979**, *100*, 745−757.

https://doi.org/10.1021/acs.jpcc.3c02830
J. Phys. Chem. C 2023, 127, 16367−16373